2 μm GaInAsSb/AlGaAsSb midinfrared laser grown digitally on GaSb by modulated-molecular beam epitaxy

C. Mourad[a)]
Center for High Technology Materials, University of New Mexico, Albuquerque, New Mexico 87106

D. Gianardi
Boeing Defense and Space Group, Albuquerque, New Mexico 87106

K. J. Malloy
Center for High Technology Materials, University of New Mexico, Albuquerque, New Mexico 87106

R. Kaspi
Air Force Research Laboratory, Directed Energy Directorate, AFRL/DELS, Kirtland Air Force Base, Albuquerque, New Mexico 87106

(Received 26 June 2000; accepted for publication 30 August 2000)

Stimulated emission at 1.994 μm was demonstrated from an optically pumped, double quantum well, semiconductor laser that was digitally grown by modulated-molecular beam epitaxy. This ''digital growth'' consists of short period superlattices of the ternary GaInAs/GaInSb and GaAsSb/GaSb/AlGaSb/GaSb alloys grown by molecular beam epitaxy with the intent of approximating the band gaps of quaternary GaInAsSb and AlGaAsSb alloys in the active region and barriers of the laser, respectively. For a 50 μs pulse and a 200 Hz repetition rate, the threshold current density was 104 W/cm^2 at 82 K. The characteristic temperature (T_0) was 104 K, the maximum operating temperature was 320 K and the peak output power was 1.895 W/facet at 82 K with pumping power of 7.83 W. © *2000 American Institute of Physics.* [S0021-8979(00)04023-8]

I. INTRODUCTION

Antimonide-based semiconductor materials[1] are important due to their potential application as semiconductor midinfrared lasers with emission wavelength in the range of 2–4 μm.[2–9] These GaSb devices are promising for a variety of military and civil applications such as infrared imaging sensors, fire detection and monitoring environmental pollution. The GaInAsSb/AlGaAsSb system has many growth problems including compositional control as well as reproducibility of the structures that are designed. Growth and compositional control of mixed anion III/V compound semiconductor alloys by solid-source molecular beam epitaxy (MBE) is extremely difficult due to the lack of unity incorporation of group V fluxes. The arsenic mole fraction that is incorporated is determined by competition which depends on the growth temperature, the III/V ratio, the As/Sb ratio and the growth rate. Abrupt compositional changes are difficult, and reproducibility within heterostructures and from run to run are poor. However, when short-period superlattices (or digital alloys) composed of binary or ternary layers of a single group V composition are used as an alternative to mixed anion random alloys, we find that the structural, optical and electronic properties are suitable substitutes for the random alloy.[10] The above-mentioned disadvantages encountered in conventional MBE growth of mixed group V alloys are minimized as well. For digital growth of $Ga_xIn_{1-x}As_ySb_{1-y}$, for example, compositional control of group V, i.e., of the As mole fraction, is achieved through control of the As shutter duty cycle where the As_2 and Sb_2 shutters are alternately modulated.[11,12]

$$\text{As mole fraction} = \text{As}_{\text{shutter time}}/(\text{As}_{\text{shutter time}} + \text{Sb}_{\text{shuttertime}}).$$

Consequently the ratio of thicknesses of the deposited layers (if the growth rates of the individual layers are assumed to be identical) can be used to deduce the composition of the alloy. Alloys grown by conventional MBE are referred to as random alloys, and those grown by modulated-MBE (MMBE) by creating short-period superlattices are referred to as digital alloys. Growing digitally by MMBE shifts the emphasis placed on control of incident fluxes (which are hard to reset in conventional MBE) to shutter timing and layer thicknesses (which are easy to control). Hence both reproducibility and compositional control difficulties are reduced.

In this article, we report results on an optically pumped quaternary GaInAsSb/AlGaAsSb[2,7,13] digital alloy laser, in which both the quantum wells and the barriers are grown digitally via MMBE.[12,11,14,15]

II. GROWTH OF THE LASER STRUCTURE

The laser structure studied was grown using a conventional solid-source MBE system and was designed for optical pumping. A schematic band diagram of the GaInAsSb/AlGaAsSb double quantum well laser is shown in Fig. 1 and it has the following nominal structure.

A 0.16 μm thick GaSb buffer layer was grown on top of an *n*-type GaSb (Te doped) substrate followed by a 1.5 μm thick randomly grown cladding layer with composition

a)Electronic mail: mourad@unm.edu

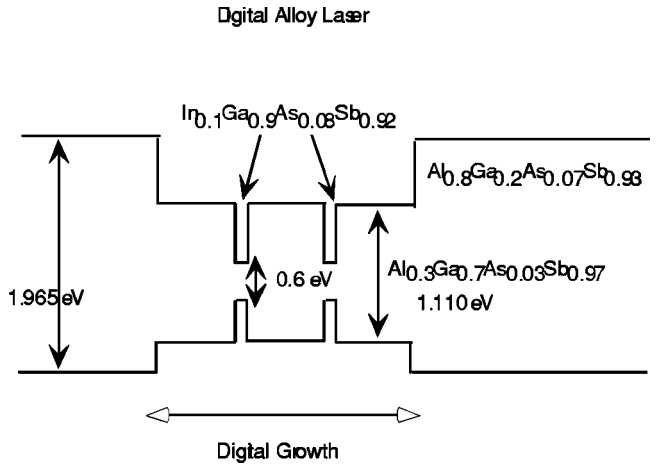

FIG. 1. Schematic energy band diagram of the double quantum well digital alloy laser structure studied.

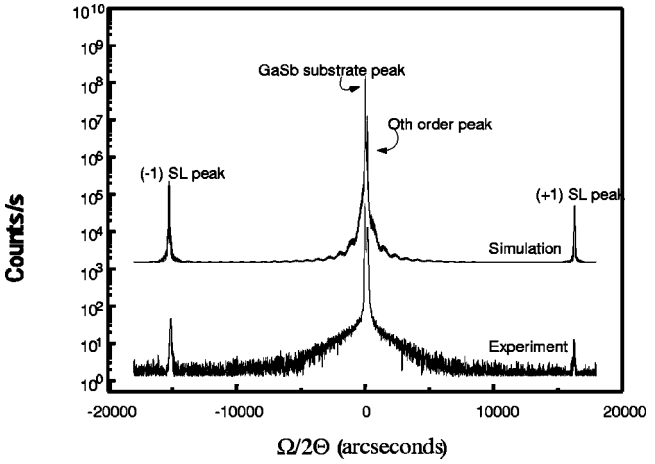

FIG. 3. 004 reflection high-resolution x-ray diffraction curve from a 3000 Å $Ga_{0.9}In_{0.1}As_ySb_{1-y}$ bulk digital alloy test structure consisting of 248 layers with composition of $Ga_{0.9}In_{0.1}As/Ga_{0.9}In_{0.1}Sb$ including a rocking curve dynamical simulation of the nominal structure.

$Al_{0.8}Ga_{0.2}As_xSb_{1-x}$. This was followed by two 150 Å quantum well regions separated by a 0.1 μm thick barrier region, all of which were digitally grown. The shutter time sequence for digital growth of the barrier region by MMBE is shown in Fig. 2, where the Al and As_2 shutters are modulated while keeping the Ga and Sb_2 shutters open. For the quantum well region only the As_2 and Sb_2 shutters are alternately modulated while the In and Ga shutters are kept open. This was followed by a 1 μm thick randomly grown cladding layer topped by a 50 Å thick GaSb cap. The barriers and quantum wells have the following compositions: $Al_{0.3}Ga_{0.7}As_ySb_{1-y}$ and $Ga_{0.9}In_{0.1}As_zSb_{1-z}$, respectively.

Prior to growth of the laser structure, the cladding layer, the quantum wells and the barriers are calibrated for the desired compositions. For the random alloy region in the cladding, the appropriate incident As_2 and Sb_2 fluxes at a given growth rate and temperature are used. For digital growth in the barriers and active regions, the incident fluxes are calibrated for the group III elements at a specific growth rate and temperature, while the group V compositions are determined by the duty cycles at the lattice-match condition. These are determined by growing several test samples with various duty cycles, and are characterized by x-ray diffraction. The duty cycles that correspond to the lattice-match condition are selected for growth of the entire structure. The attractiveness of the digital alloy growth technique by MMBE lies in the fact that only the shutter time sequences will determine the compositions of the barrier and quantum well regions and the entire structure is grown without variation of the incident fluxes.

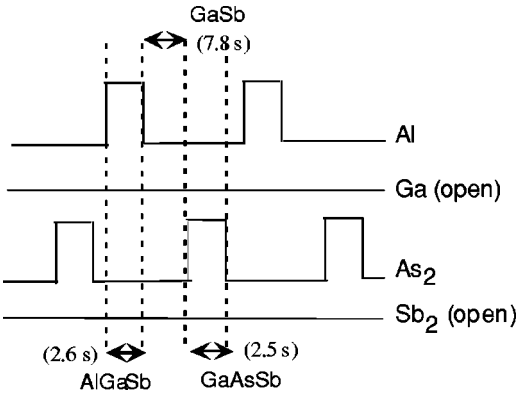

FIG. 2. Schematic time shutter sequence utilized during MMBE growth of the AlGaAsSb digital alloy barrier region of the laser structure lattice matched to GaSb.

The procedure for digital growth is as follows: the barriers are grown at 550 °C at a 6 monolayer (18.3 Å) periodicity with the alloy consisting of layers of GaAsSb (2.5 s)/GaSb (7.8 s)/GaAlSb (2.6 s)/GaSb (3.8 s) to produce an average composition of $Al_{0.3}Ga_{0.7}As_{0.03}Sb_{0.97}$ shown in Fig. 2. This shutter sequence was repeated 55 times to grow a 0.1 μm thick barrier and is one possible sequence among numerous ones making the digital alloy technique flexible. The quantum wells are digitally grown at 440 °C with a periodicity of 4 monolayers (ML) (12.2 Å) consisting of 2 ternary layers $Ga_{0.9}In_{0.1}As$ (2.5 s) and $Ga_{0.9}In_{0.1}Sb$ (4.3 s), grown at 0.59 ML/s, and 12 repetitions to grow a 150 Å thick layer. The laser structure is composed of a total of 710 layers.

III. STRUCTURAL AND OPTICAL PROPERTIES

The structural properties of the laser are studied noninvasively via high-resolution x-ray diffraction (HRXRD) with a Philips double-crystal x-ray diffractometer that utilizes the Cu K_{α_1} line after four symmetric 022 reflections on the surfaces of four Ge crystals (four crystal Bartel's monochromator) and no receiving slits (open face detector mode). Figure 3 shows a symmetric experimental and theoretical dynamical simulation[16] of the 004 reflection $\Omega/2\theta$ x-ray diffraction scan of a 3000 Å thick bulk $Ga_{0.9}In_{0.1}As_ySb_{1-y}$ digital alloy test structure, lattice matched to GaSb (001) which has the same periodicity and composition as the quantum wells of the laser structure. Distinct satellite peaks corresponding to a short-period superlattice with a period of 11.7 Å are observed, which is consistent with the nominal periodicity of 12.2 Å, indicating the high structural quality obtained from this digital alloy growth. The lattice mismatch of the

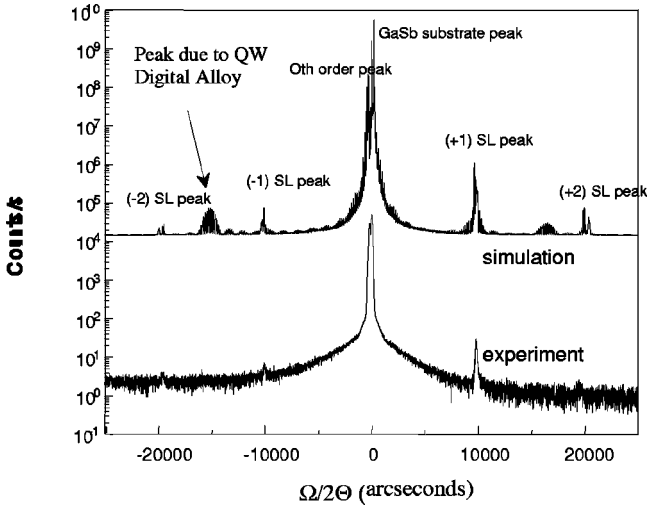

FIG. 4. 004 reflection high-resolution x-ray diffraction curve from the 710 layer double quantum well digital alloy laser structure with a simulation of the nominal structure.

$Ga_{0.9}In_{0.1}As_ySb_{1-y}$ digital alloy to the GaSb substrate is less than 9.2×10^{-4}. The zeroth-order peak has a full width at half maximum (FWHM) of 108 arcsec and the GaSb substrate a FWHM of 82.8 arcsec.

In Fig. 4, a symmetric 004 reflection $\Omega/2\theta$ x-ray diffraction spectrum of the more complex digital alloy laser structure is shown. We can clearly observe two orders of the superlattice digital alloy Bragg peaks corresponding to a periodicity of 19.1 Å. This agrees well with the nominal barrier periodicity of 18.3 Å. The lattice mismatch of the spacer layer $Al_{0.8}Ga_{0.2}As_ySb_{1-y}$ to the substrate is 0.296×10^{-2}. The FWHM of the zeroth-order is 176.4 arcsec and that of the substrate is 158.4 arcsec. Also plotted in Fig. 4 is a rocking curve simulation of the nominal structure, where two orders of the superlattice peaks are observed at the expected positions. However, two extra peaks due to quantum well digital alloy periodicity are also observed in the simulation but not experimentally since these peaks have weak intensities and fall below the noise level of the diffractometer.

The optical properties of the material are characterized using a continuous wave (cw) Ti:sapphire laser with pump wavelength of 700 nm, and an InSb detector to record the photoluminescence (PL) intensity and wavelength. A single PL peak at 1941 nm with two shoulders at 1798 and 1710 nm are observed. The main peak corresponds to the recombination between the first electron subband and the first heavy-hole subband (C-HH_1) and has a FWHM of 35.5 meV. Comparison with theoretical calculations indicates that the shoulder at 1798 nm is likely to be due to transitions involving light holes (C-LH_1), and the shoulder at 1710 nm corresponds to the GaSb substrate band gap. These results are indicative of the good optical quality of the laser material, as well as of the material producing the expected optical wavelength.

IV. LASER RESULTS AND DISCUSSION

A 2.55 mm digital alloy laser cavity was pumped using an 808 nm pump array pulsed at a 1% duty cycle, 200 Hz repetition rate and a duration of 50 μs. The excitation stripe of the focused pump light was estimated to be 250 μm. Figure 5 shows $L-L$ curves obtained from optically pumping the laser cavity at operating temperatures varying from 82 to 320 K. The differential quantum efficiency η_d for optically pumped lasers is

$$\eta_d(T)=\frac{\Delta P_{\text{out}}(T)}{\Delta P_{\text{in}}}\frac{\lambda_{\text{out}}(T)}{\lambda_{\text{pump}}},$$

where $\lambda_{\text{pump}}=808$ nm is the pump wavelength, λ_{out} is the emitting wavelength in nm and $\Delta P_{\text{out}}/\Delta P_{\text{in}}$ is the differential slope efficiency of the $L-L$ curve at a particular operating temperature. The differential quantum efficiency is 48%/facet at 82 K. A characteristic temperature T_1 using $\eta_d=\eta_{d_0}e^{(-T/T_1)}$ is obtained. The T_1 value of 77 K (shown in Fig. 6) indicates that the differential quantum efficiency η_d falls off rapidly at higher temperatures due to the onset of internal losses, which are influenced by defects and nonradiative regions where Auger recombination processes dominate.[17] The peak output power measured is 1.895 W/facet at 82 K and the pumping peak power is 7.83 W. At maximum pumping power no catastrophic degradation of the device is observed. Therefore, it is reasonable to believe that

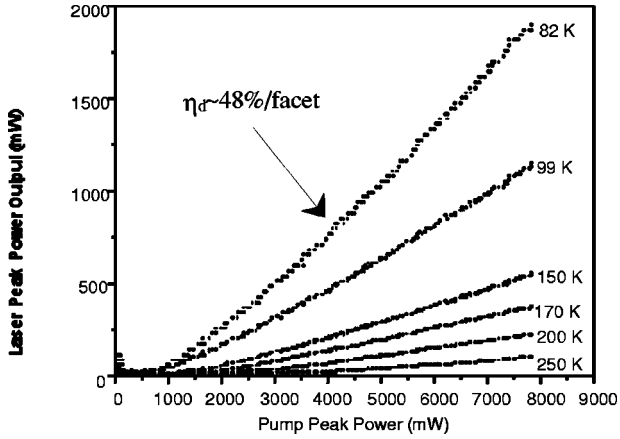

FIG. 5. $L-L$ curves of the laser at increasing operating temperatures.

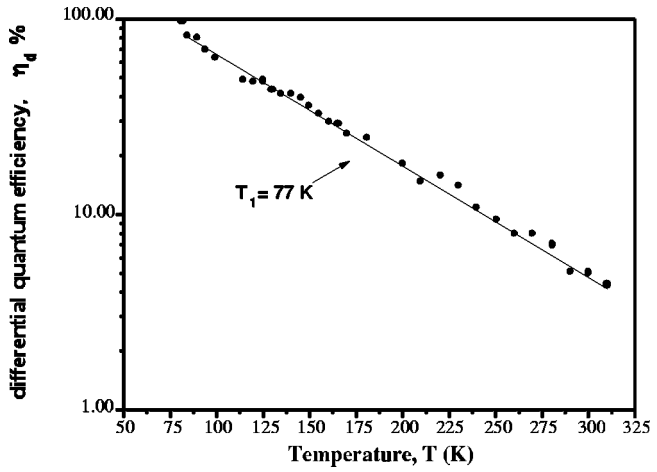

FIG. 6. Differential quantum efficiency η_d vs operating temperature of the laser.

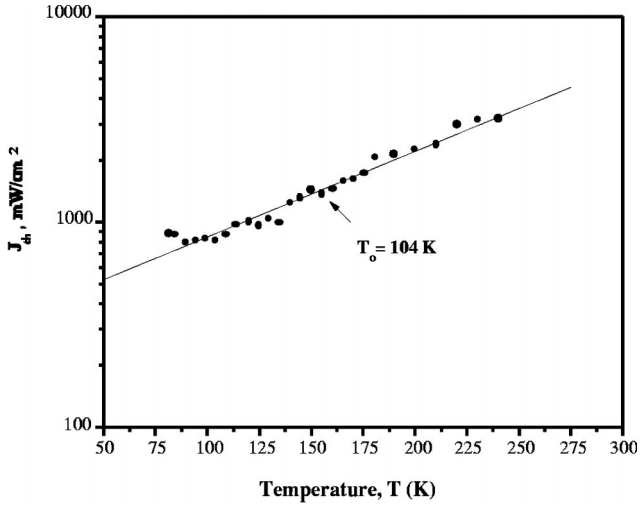

FIG. 7. Threshold current densities J_{th} vs operating temperature of the laser.

a higher maximum peak power could be achieved using even higher pumping power. It is also observed that the threshold current density is low at $\sim$104 W/cm^2, which is approximately equivalent to 148 A/cm^2 for an electrically injected laser at 82 K. Figure 7 shows the characteristic temperature T_0 calculated for the laser using the equation $J_{th} = J_0 e^{(T/T_0)}$. The T_0 is 104 K (Fig. 7), which is comparable to 113 K obtained for 2.1 μm diode lasers[2] and 140 K for a four quantum well electrically pumped laser.[18] However this is larger than the 65 K obtained for 2 μm optically pumped double heterostructure (DH) lasers grown by liquid phase epitaxy (LPE)[13] and 49 K for 2.2 μm diode lasers grown by MBE.[4] The laser operates up to 320 K, with the laser mode shifting at a rate $\sim$0.88 nm/K below 200 K, and at $\sim$1.15 nm/K above 200 K.

V. CONCLUSIONS

In this article, we have reported on a GaInAsSb/AlGaAsSb double quantum well digital alloy laser, in which the digital alloy approach by modulated-MBE has been used to build strain compensated very short-period superlattices to replace conventionally MBE-grown mixed group V random alloys. The intent was to create digital alloys that have band gaps equivalent to conventional randomly grown quaternary GaInAsSb and AlGaAsSb alloys. This technique is beneficial from the growth point of view, where the incident fluxes remain unaltered, and compositions are controlled well simply by varying the shutter sequence of the effusion cells, hence minimizing many growth problems encountered in the growth of mixed As/Sb mixed alloys. From HRXRD and PL data, there is evidence that the laser is of high structural and optical quality. Well defined digital alloy superlattice Bragg peaks corresponding to periodicity as small as 4 ML and a PL peak at the expected wavelength of 1941 nm at room temperature are observed. When the laser was tested, we discovered that the optically pumped laser has a T_0 comparable to that found in the literature for other mid-IR lasers. The laser operates up to 320 K, the threshold current density is small at 104 W/cm^2 and has a high power output of 1.895 W/facet at 82 K. These results demonstrate the applicability of the digital alloying technique to complex heterostructure optoelectronic devices in which a large number of layers ($\sim$710) have been grown.

ACKNOWLEDGMENTS

The authors would like to thank the Phillips Labs/LIDA group at Kirtland Air Force Base for their support, in particular Dr. A. Ongstad and C. Moeller for useful discussions and for help in the laser measurements. Dr. G. T. Liu is also to be thanked for his assistance in the PL measurements.

[1] H. L. Bhat, P. S. Dutta, and V. Kumar, J. Appl. Phys. **81**, 5821 (1997).
[2] S. J. Eglash and H. K. Choi, Appl. Phys. Lett. **61**, 1154 (1992).
[3] R. U. Martinelli, D. Z. Garbuzov, H. Lee, P. K. York, R. J. Menna, J. C. Connolly, and S. Y. Narayan, Appl. Phys. Lett. **69**, 2006 (1996).
[4] H. K. Choi and S. J. Eglash, Appl. Phys. Lett. **59**, 1165 (1991).
[5] H. K. Choi, G. W. Turner, and M. J. Manfra, Appl. Phys. Lett. **72**, 876 (1997).
[6] H. Temkin, B. V. Dutt, E. D. Kolb, and W. A. Sunder, Appl. Phys. Lett. **47**, 111 (1985).
[7] H. K. Choi and S. J. Eglash, IEEE J. Quantum Electron. **27**, 1555 (1991).
[8] C. H. Lin, S. S. Pei, and H. Q. Le, Appl. Phys. Lett. **72**, 3434 (1998).
[9] S. J. Eglash and H. K. Choi, Appl. Phys. Lett. **64**, 833 (1994).
[10] C. Mourad, Ph.D. thesis, University of New Mexico, Albuquerque, NM, 2000.
[11] Y.-H. Zhang and D. H. Chow, Appl. Phys. Lett. **65**, 3239 (1994).
[12] Y.-H. Zhang, J. Cryst. Growth **150**, 838 (1995).
[13] Y. Zhao, A. Z. Li, Y. L. Zheng, G. T. Chen, G. P. Ru, W. Z. Shen, and J. Q. Zhong, J. Cryst. Growth **175/176**, 873 (1997).
[14] J. Y. Marzin, B. Jusserand, and J. M. Gerard, J. Cryst. Growth **111**, 205 (1991).
[15] H. Q. Le, Y. H. Zhang, D. H. Chow, and R. H. Miles, Inst. Phys. Conf. Ser. (unpublished).
[16] Bede Scientific Instruments Ltd., Rocking Curve Analysis by Dynamical Simulation, Windows Ver. 3.00, UK, 1998.
[17] J. R. Meyer *et al.*, Appl. Phys. Lett. **68**, 2976 (1996).
[18] X. Wu, T. Newell, A. L. Gray, S. Dorato, H. Lee, and L. F. Lester, IEEE Photonics Technol. Lett. **11**, 30 (1999).